DRAFT VERSION DECEMBER 9, 2016
Preprint typeset using LaTeX style AASTeX6 v. 1.0

arXiv:1612.02815v1 [astro-ph.GA] 8 Dec 2016

RECALIBRATION OF THE $M_{BH} - \sigma_\star$ RELATION FOR AGN

MERIDA BATISTE[1], MISTY C. BENTZ[1], SANDRA I. RAIMUNDO[2], MARIANNE VESTERGAARD[2,4], CHRISTOPHER A. ONKEN[3]

[1]Department of Physics & Astronomy, Georgia State University, 25 Park Place, Atlanta, GA 30303, USA; batiste@astro.gsu.edu
[2]Dark Cosmology Centre, Niels Bohr Institute, University of Copenhagen, Juliane Maries Vej 30, DK-2100 Copenhagen Ø, Denmark
[3]Research School of Astronomy & Astrophysics, The Australian National University, Canberra, ACT 2611, Australia
[4]Department of Astronomy and Steward Observatory, University of Arizona, 933 N. Cherry Avenue, Tucson, AZ

ABSTRACT

We present a re-calibration of the $M_{BH} - \sigma_\star$ relation for AGN, based on a sample of 16 reverberation-mapped galaxies with newly determined bulge stellar velocity dispersions ($\sigma_\star$) from integral-field (IFU) spectroscopy. IFU spectroscopy provides a spatially resolved view of the stellar kinematics within the bulge of each target galaxy, from which significantly improved $\sigma_\star$ determinations can be made. This method accounts for variations in the stellar kinematics resulting from the presence of substructure (e.g. bars), and avoids many of the biases that are known to be present in long slit and single aperture spectroscopy. The sample covers three orders of magnitude in black hole mass, and is approximately evenly split between early- and late-type galaxies, and barred and unbarred galaxies. We find a best fitting slope of $\beta = 3.77 \pm 0.99$ for the full sample, which is consistent with recent estimates of the relation for active galaxies, and shallower than recent estimates of the relation for quiescent galaxies. We find that our best-fit relationship is not sensitive to galaxy morphology. We recalculate the virial scaling factor f required to bring the reverberation-mapped AGN sample into agreement with the fit for quiescent galaxies, and find $f = 3.39 \pm 1.28$.

Keywords: galaxies: active — galaxies: kinematics and dynamics — galaxies: bulges

1. INTRODUCTION

A wealth of observational evidence demonstrates that the formation and evolution of galaxies and their central supermassive black holes (BHs) are fundamentally connected. This physical connection is exemplified by empirically determined scaling relations between the mass of a central black hole, M_{BH}, and numerous properties of the host galaxy, including the bulge stellar velocity dispersion, $\sigma_\star$ (Ferrarese & Merritt 2000; Gebhardt et al. 2000). These scaling relations provide insight into the mechanisms governing the formation and evolution of structure, and may be used to estimate M_{BH} for large samples of galaxies at cosmological distances. Thus they are essential tools in probing the evolution of structure across cosmic time.

Accurate calibration of scaling relations requires a sample of galaxies with secure M_{BH} determinations. In quiescent galaxies this is usually done by modeling the spatially resolved gas and stellar kinematics within the gravitational sphere of influence of the black hole, and is thus limited to the local universe. To probe M_{BH} over cosmological distances one must use active galaxies, for which M_{BH} can be determined from the active galactic nucleus (AGN) via reverberation-mapping (RM) (Blandford & McKee 1982). RM exploits the variability of the AGN to probe the gas in the broad-line region (BLR) around the black hole. A dimensionless scale factor f is necessary for this method, to account for the unknown geometry and kinematics of the BLR. Since direct determination of f is not feasible in most cases, it is assumed that AGN and quiescent galaxies follow the same $M_{BH} - \sigma_\star$ relation. The value of f is then estimated as the average multiplicative offset that is required to bring the relation for AGN and quiescent galaxies into agreement (Onken et al. 2004). Accurate calibration of the $M_{BH} - \sigma_\star$ relation is, therefore, essential for RM M_{BH} determinations.

The $M_{BH} - \sigma_\star$ relation appears to be the tightest, and arguably the most fundamental, of the observed scaling relations (Beifiori et al. 2012; Shankar et al. 2016), and has consequently been the subject of extensive investigation (see reviews by Kormendy & Ho 2013, and Graham 2016). In spite of this it is still unclear what the actual best-fitting relation is, or indeed whether a single relation holds for both active and quiescent galaxies. While some studies have shown a significant difference between the slope of the relation for quiescent galaxies (McConnell & Ma 2013) and AGN (Woo et al. 2010), which may critically impact the scaling of all RM M_{BH}, other investigations indicate that this difference may simply be an artifact of sample selection bias (Woo et al. 2013).

Studies have also suggested a morphological dependence

of the $M_{BH} - \sigma_\star$ relation. In particular, there is evidence that galaxies with substructure such as bars and pseudo-bulges are offset from the elliptical-only relation, and tend to increase the scatter (e.g. Graham 2008; Hu 2008; Gültekin et al. 2009). This is of particular relevance when making $\sigma_\star$ determinations for RM AGN, which is often done via single aperture and long-slit spectroscopy. In most cases contamination by dynamically distinct substructure is unavoidable, and disk contamination is a particular problem for single aperture spectra, where rotational broadening has been observed to significantly affect $\sigma_\star$ if corrections are not applied (e.g. Graham et al. 2011; Woo et al. 2013; Hartmann et al. 2014; Bellovary et al. 2014). In addition, Batiste et al. (2016) showed that the effect of slit orientation, relative to substructure such as bars, can strongly impact the measured $\sigma_\star$. These issues preferentially impact the spiral dominated local RM AGN sample, thereby inhibiting investigation of possible differences between quiescent and active galaxies.

This problem is at least somewhat mitigated by spatially resolved kinematics, and the recent proliferation of integral-field (IFU) spectrographs allows for significant improvement in $\sigma_\star$ determinations for the RM AGN sample. We have made new $\sigma_\star$ estimates, based on IFU spectra, for ten AGN with secure RM M_{BH} determinations (Batiste et al. 2016), and IFU data are available in the literature for a further six. In this letter we use this sample of 16 galaxies with newly determined $\sigma_\star$ to re-calibrate the $M_{BH} - \sigma_\star$ relation for AGN, and provide a new estimate of the scale factor f for use with RM M_{BH} determination. Throughout this work we adopt a ΛCDM cosmology with $\Omega_m = 0.3$, $\Omega_\Lambda = 0.7$, and $H_0 = 70\,\mathrm{km\,s^{-1}\,Mpc^{-1}}$.

2. DATA

2.1. *Virial Products from Reverberation-Mapping*

RM allows for accurate determination of the virial product (VP), given by $\mathrm{VP} = V^2 R_{BLR}/G$, where G is the gravitational constant, V is measured from the width of a broad emission line, and R_{BLR} is the size of the BLR. VPs for the 16 galaxies in our sample are shown in column (7) of Table 1. These are all taken from the AGN Black Hole Mass Database[1] (Bentz & Katz 2015) with the exception of MCG 06-30-15, for which the VP is taken from the work of Bentz et al. (2016a). In all cases, VP is determined from the H_β line. References for the individual measurements from which the VPs are determined are available from the database.

2.2. *Stellar Velocity Dispersion Maps*

Spatially resolved stellar kinematics are available for ten RM AGN host galaxies from the work of Batiste et al. (2016). Details of the observations, data reduction, and analysis are given in that paper, so we review only briefly here.

Observations of eight galaxies were made with the HexPak optical IFU (Wood et al. 2012) on the WIYN 3.5m telescope at Kitt Peak National Observatory. HexPak has a unique design, with a hexagonal field of view (FoV) $40\farcs9 \times 35\farcs8$ consisting of 102 fibers of variable pitch. A central bundle of $0\farcs94$ fibers covers the central $6''$ of the FoV, surrounded by a hexagonal array of $2\farcs9$ fibers. This design provides high spatial resolution in the bright central region of a galaxy, while providing approximately constant S/N across the FoV.

Observations of NGC 6814 were made with the Wide-Field Spectrograph (WiFeS) optical IFU on the ANU 2.3m telescope at Siding Spring Observatory (Dopita et al. 2007, 2010). WiFeS has a similar FoV to HexPak, $25'' \times 38''$, with $1'' \times 0\farcs5$ spaxels that were binned to provide $1''$ square spatial sampling.

Observations of Mrk 79 taken with Gemini-North's Near-infrared Integral Field Spectrometer (NIFS, McGregor et al. 2003) were available from the Gemini Observatory Archive[2]. NIFS has a much smaller FoV than either HexPak or WiFeS, $3'' \times 3''$, with $0\farcs1$ spatial resolution facilitated by adaptive optics.

For the galaxies observed with HexPak and WiFeS the kinematics are mapped well beyond the bulge effective radius (r_e), into the disk of each galaxy. While the FoV afforded by NIFS is substantially smaller than that of HexPak or WiFeS, Mrk 79 is more distant so the kinematics are mapped out to $\sim r_e/2$.

In all cases, data were reduced following standard procedures for IFU spectrographs. Stellar kinematics were determined using the penalized pixel-fitting method (pPXF) of Cappellari & Emsellem (2004), which employs a user-defined set of stellar template spectra to model the line-of-sight velocity distribution of the galaxy spectrum. This is done for each spectrum obtained with the IFU, providing spatially resolved maps of the stellar kinematics for each galaxy, which are presented by Batiste et al. (2016).

2.2.1. *NGC 5273*

IFU observations of NGC 5273 were obtained as part of the ATLAS^{3D} survey of early-type galaxies in the northern hemisphere (Cappellari et al. 2011). Observations were made with the SAURON optical IFU (Bacon et al. 2001) on the William Herschel Telescope at the Observatory of El Roque des Los Muchachos on La Palma. Low-resolution mode was used, providing a $33'' \times 44''$ FoV with $0\farcs94$ spatial sampling. Details of the observations and data reduction are presented by Cappellari et al. (2011).

Fully reduced and analyzed data for the galaxies included in the ATLAS^{3D} project are publicly available[3] and so we have chosen to make use of their available kinematics, which

[1] http://www.astro.gsu.edu/AGNmass/

[2] https://archive.gemini.edu/

[3] http://www-astro.physics.ox.ac.uk/atlas3d/

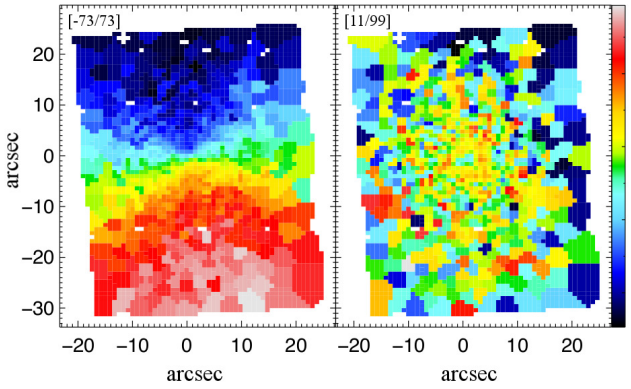

Figure 1. Maps of velocity (left) and stellar velocity dispersion ($\sigma_\star$, right) for NGC 5273. The range of plotted values is shown in the top left corner of each map.

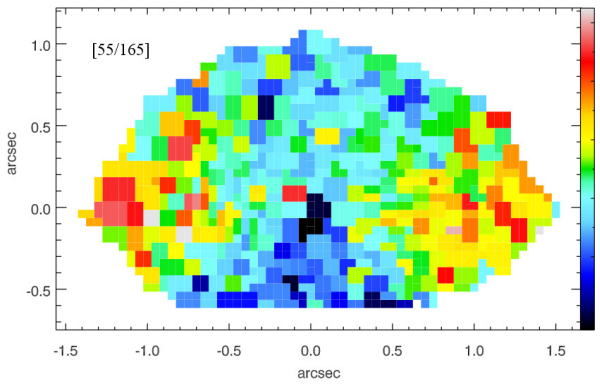

Figure 2. Map of stellar velocity dispersion ($\sigma_\star$) for MCG 06-30-15, based on data first presented by Raimundo et al. (2013), with the range of plotted values shown in the top left corner.

were determined using pPXF. Details of the analysis are presented by Krajnović et al. (2011) and Cappellari et al. (2013). Kinematic maps based on the publicly available data are shown in Figure 1.

2.2.2. *MCG 06-30-15*

The first near-IR IFU spectroscopy observations of MGC 06-30-15 were presented by Raimundo et al. (2013). The data were obtained with the SINFONI IFU on the VLT (Eisenhauer et al. 2003; Bonnet et al. 2004), which has a FoV $3'' \times 3''$ and for which adaptive optics afford a spatial resolution of $\sim 0\farcs1$.

Stellar kinematics were determined using pPXF, and details of the observations, data reduction and analysis are presented by Raimundo et al. (2013). The spatially resolved map of $\sigma_\star$, based on that analysis, is shown in Figure 2.

2.3. *Bulge Effective Radii*

Accurate determinations of r_e are available for all of the galaxies that have been discussed, from the works by Bentz et al. (2009, 2013, 2014, 2016a) and Bentz et al. (in prep). In all cases, r_e are determined from detailed models of surface brightness decompositions of Hubble Space Telescope (HST) images, made using GALFIT (Peng et al. 2002, 2010). These models account for the bright central AGN, isolating it from the galaxy surface brightness features, as well as for substructure such as bars and disks. Table 1 shows r_e for each galaxy in the sample, along with the relevant reference in which full details of the method can be found.

2.4. *Bulge Stellar Velocity Dispersions*

Following the method described by Batiste et al. (2016), $\sigma_\star$ is determined by taking an error weighted average of the values for each spaxel within r_e. This value is shown for each galaxy in column (4) of Table 1. In the case of Mrk 79, r_e is not completely covered by the NIFS FoV, so an aperture correction is applied to determine the average $\sigma_\star$ within r_e (van den Bosch 2016):

$$\frac{\sigma_{\star_e}}{\sigma_\star} = \left(\frac{r_{NIFS}}{r_e}\right)^{0.08} \quad (1)$$

In the case of MCG-06-30-15, we follow Raimundo et al. (2013) and exclude the central $0\farcs1$ from our calculation of $\sigma_\star$, as the noise associated with the AGN continuum precludes secure measurement of the stellar kinematics in these spaxels. In addition, it can be seen in Figure 2 that a small portion of the region within r_e ($1\farcs014$) was cut off ($y \leq -0\farcs6$). This was due to an illumination artifact present in the SINFONI data which caused a $\sim 0\farcs3$ wide region, parallel to the major axis of the galaxy and at $\sim 0\farcs8$ from the center of the FoV, to have to be removed. We have assumed that the kinematics within r_e are nonetheless well represented by the region within the FoV, and have thus determined $\sigma_\star$ without correcting for the absence of this region. As a check on this assumption we have also determined $\sigma_\star$ within a smaller aperture of $0\farcs6$, which is completely contained within the field, and then applied equation 1 to correct to r_e. These values differ by less than $1\ \mathrm{km\ s^{-1}}$, so we consider the original determination to be an adequate approximation.

Two estimates of uncertainty are provided for each $\sigma_\star$ determination. The statistical uncertainty, based on the measurement error, is shown in column (4) of Table 1 along with $\sigma_\star$. Column (5) shows the standard deviation for the set of $\sigma_\star$ values averaged to determine the overall $\sigma_\star$ value (quoted in column 4). The standard deviation quantifies somewhat the spatial variation in the kinematics within r_e, and thus may be more physically meaningful as an estimate of uncertainty.

Additionally, $\sigma_\star$ determinations from IFU data are available for 4 high-luminosity quasar hosts from Grier et al. (2013). Unlike the observations that have so far been discussed, stellar kinematics for these targets were determined from single spectra. Spectra from individual spaxels, within an annulus that removed the central spaxels dominated by AGN emission, were integrated to obtain the final galaxy spectrum from which stellar kinematics were determined. In

each case the (maximum) radius of the aperture within which the spectrum was integrated was varied, in order to maximize host galaxy S/N. Consequently, the $\sigma_\star$ values quoted by Grier et al. (2013) are not determined within r_e. We therefore apply the aperture correction shown in equation 1 to the quoted $\sigma_\star$ for each of these galaxies, to determine the $\sigma_\star$ shown in Table 1.

3. THE $M_{BH} - \sigma_\star$ RELATION

The $M_{BH} - \sigma_\star$ relation is given by:

$$\log\left(\frac{\mathrm{M_{BH}}}{\mathrm{M_\odot}}\right) = \alpha + \beta \log\left(\frac{\sigma_\star}{200\ \mathrm{km\ s^{-1}}}\right) \quad (2)$$

The sample of galaxies listed in Table 1 is used to determine the best-fitting slope of this relation for AGN, where VP is used in place of M_{BH} (since $M_{BH} = f$ VP, the offset determined from this fitting is then $\alpha - \log f$). This is done by fitting a standard forward regression using the LINMIX_ERR routine of Kelly (2007), which employs a fully Bayesian approach. For comparison, the popular MPFITEXY routine of Williams et al. (2010) is also used. Park et al. (2012) tested these fitting routines and found them to be similarly robust and unbiased, however they also found that LINMIX_ERR provides more reliable uncertainties in all parameters, so we adopt these results as our best fit. Since we have two error estimates for $\sigma_\star$ (except for those taken from the analysis of Grier et al. 2013, for which only the quoted measurement error is used), the relation is fit with both sets, though we follow convention and adopt as our best fit that which uses the statistical error (given in column (4) of Table 1).

The best fit parameters determined via these routines are shown in Table 2, and differ only marginally. In general the fits that take the standard deviation (column (5) of Table 1) as the error in $\sigma_\star$ are steeper, however they are all fully consistent with each other. The best fitting relation is given by:

$$\log\left(\frac{\mathrm{VP}}{\mathrm{M_\odot}}\right) = (7.48\pm0.27)+(3.77\pm0.99)\log\left(\frac{\sigma_\star}{200\ \mathrm{km\ s^{-1}}}\right) \quad (3)$$

This agrees with the best fit for RM AGN found by Woo et al. (2013) ($\beta = 3.46\pm0.61$), as well as for two of their quiescent galaxy subsamples: late-type galaxies ($\beta = 4.23\pm1.26$), and galaxies with pseudo-bulges ($\beta = 3.28\pm1.11$). This slope is shallower than, but consistent with, that of Kormendy & Ho (2013) ($\beta = 4.38 \pm 0.29$), and it is shallower than that found by Grier et al. (2013) ($\beta = 5.04 \pm 0.19$), as well as that of Savorgnan & Graham (2015) ($\beta = 6.34 \pm 0.8$). The scatter in the relation is found to be 0.35 ± 0.17, which is completely consistent with the studies that have been mentioned here.

In order to recalculate the virial scale factor f, we adopt the fit of Woo et al. (2013) for quiescent galaxies, with $\beta = 5.31$ and $\alpha = 8.37$, and determine the value needed to bring our AGN sample into agreement with their quiescent galaxy sample. We use an adapted version of LINMIX_ERR that makes it possible to fix the slope, and find $\log f = 0.53 \pm 0.16$, giving $f = 3.39 \pm 1.28$. Column (5) of Table 2 shows $\log f$ determined with each estimate of uncertainty, and for the two fitting routines. When the standard deviation is used rather than the statistical error, we find a slightly higher value of $f = 3.52 \pm 1.32$, but these two values are completely consistent. Our calculated f is slightly lower than, but consistent with, recent estimates (e.g. Graham et al. 2011; Grier et al. 2013; Woo et al. 2013, 2015). It is also consistent with the results of direct modeling of the BLR by Pancoast et al. (2014), who modeled five active galaxies (including NGC 5548 and NGC 6814, which are included in this sample) and determined separate f values for each, finding a mean value of $\langle \log f \rangle = 0.68 \pm 0.40$.

Our calculated f value is significantly lower than the original determination of $f = 5.5$, presented by Onken et al. (2004). There are a number of possible explanations for this, resulting from the differences between the samples used in the two studies, and the methods by which f has been determined. VPs for all RM AGN have been significantly refined and revised over the last decade, and indeed a direct comparison between VPs for the seven galaxies that are common to the two samples demonstrates this (e.g. for NGC 3227 Onken et al. (2004) used VP $= 0.767 \times 10^7$ M$_\odot$, compared with VP $= 0.139 \times 10^7$M$_\odot$ in our sample). As has been discussed, the $\sigma_\star$ determinations for the current sample have also been significantly revised, and in some cases our value is substantially lower (e.g. for NGC 3516 Onken et al. (2004) use $\sigma_\star = 164$ km s^{-1}, compared with $\sigma_\star = 138$ km s^{-1} in our sample). Moreover the best fit for quiescent galaxies of Woo et al. (2013), which we use here, is quite significantly different to those used by Onken et al. (2004) ($\beta = 4.58$ and $\beta = 4.02$). This combination of differences and refinements is likely the dominant driver of the different f values.

Figure 3 shows the $M_{BH} - \sigma_\star$ relation for the sample (where M_{BH} is determined using $f = 3.39$), with our calculated best fit shown as a dashed line, and the fit for quiescent galaxies shown as a dotted line. Since a number of studies have suggested a morphological dependence in the $M_{BH} - \sigma_\star$ relation (see discussion in Section 1), we split the sample into early- and late-type galaxies (left panel of Figure 3), and barred and unbarred galaxies (right panel). We find no difference between these subsamples, and see no indication that barred or late-type galaxies are offset from the relation for classical spheroids. The plots may indicate higher scatter at the low mass end of the relation, which is dominated by barred and late-type galaxies in this sample, however this may well be a result of small number statistics at the high mass end. A larger sample of active galaxies with IFU observations, particularly at the high mass end, is necessary for more detailed investigation.

4. SUMMARY

Table 1. Host galaxy $\sigma_\star$ and BH VPs for the sample

Object	r_e	Ref.	$\sigma_\star$	std deviation	Ref.	VP
	($''$)		(km s^{-1})	(km s^{-1})		(10^7 $M_\odot$)
(1)	(2)	(3)	(4)	(5)	(6)	(7)
Mrk 79	2.0	1	120 ± 9	21	6	$0.951^{+0.267}_{-0.256}$
NGC 3227	2.7	5	114 ± 3	13	6	$0.139^{+0.029}_{-0.032}$
NGC 3516	2.1	5	139 ± 4	12	6	$0.577^{+0.051}_{-0.076}$
NGC 4051	1.0	5	74 ± 2	4	6	$0.031^{+0.010}_{-0.009}$
NGC 4151	2.1	5	105 ± 5	15	6	$0.923^{+0.163}_{-0.115}$
NGC 4253	1.4	2	84 ± 4	9	6	$0.032^{+0.028}_{-0.028}$
NGC 4593	11.5	5	113 ± 3	14	6	$0.177^{+0.038}_{-0.038}$
NGC 5273	6.8	3	62 ± 1	9	8	$0.103^{+0.057}_{-0.076}$
Mrk 279	1.6	1	153 ± 7	26	6	$0.657^{+0.177}_{-0.177}$
PG 1411+442	3.1	1	208 ± 30	-	7	$6.263^{+3.344}_{-3.376}$
NGC 5548	11.2	5	131 ± 3	34	6	$1.212^{+0.052}_{-0.050}$
PG 1617+175	1.7	1	201 ± 37	-	7	$9.620^{+4.272}_{-4.790}$
NGC 6814	1.7	2	71 ± 3	5	6	$0.336^{+0.063}_{-0.064}$
Mrk 509	2.8	1	183 ± 12	-	7	$2.529^{+0.223}_{-0.204}$
PG 2130+099	0.32	1	165 ± 19	-	7	$0.630^{+0.086}_{-0.086}$
MCG 06-30-15	1.014	4	102 ± 1	19	8	$0.037^{+0.010}_{-0.009}$

References. (1) Bentz et al. 2009; (2) Bentz et al. 2013; (3) Bentz et al. 2014; (4) Bentz et al. 2016a; (5) Bentz et al. 2016b; (6) Batiste et al. 2016; (7) Grier et al. 2013; (8) this work

Notes. Column 1: galaxy name, Column 2: r_e, Column 3: reference for Column 2, Column 4: $\sigma_\star$ within r_e with associated 1σ uncertainty, Column 5: standard deviation for the set of $\sigma_\star$ values averaged to determine the value in column 4. No value is included for galaxies where an integrated spectrum was used, Column 6: reference for the value in column 4, Column 7: VP taken from the AGN Black Hole Mass Database, with $f = 1$.

Table 2. Fits to the $M_{BH} - \sigma_\star$ relation

Method	$\sigma_\star$ error	α	β	log f	ϵ
(1)	(2)	(3)	(4)	(5)	(6)
LINMIX_ERR	measurement error	7.48 ± 0.27	3.77 ± 0.99	-	0.35 ± 0.17
LINMIX_ERR	standard deviation	7.51 ± 0.27	3.95 ± 1.01	-	0.31 ± 0.18
MPFITEXY	measurement error	7.44 ± 0.21	3.64 ± 0.81	-	0.45
MPFITEXY	standard deviation	7.52 ± 0.21	3.98 ± 0.78	-	0.45
LINMIX_ERR	measurement error	7.84 ± 0.16	5.31	0.53 ± 0.16	0.39 ± 0.18
LINMIX_ERR	standard deviation	7.82 ± 0.16	5.31	0.55 ± 0.16	0.31 ± 0.17
MPFITEXY	measurement error	7.81 ± 0.13	5.31	0.56 ± 0.13	0.52
MPFITEXY	standard deviation	7.82 ± 0.14	5.31	0.55 ± 0.14	0.53

Notes. Column 1: the fitting algorithm used, Column 2: the uncertainty in $\sigma_\star$ used to determine the fit, Column 3: the intercept for each fit, Column 4: the slope for each fit, Column 5: log f determined from the fit, and Column 6: scatter in the fit. The first four rows show the fits where the slope is allowed to vary, the last four rows show the fits where the slope is held fixed and from which log f can be determined.

We have presented a re-calibration of the $M_{BH} - \sigma_\star$ relation for RM AGN, using a sample of 16 galaxies with $\sigma_\star$ determinations from IFU spectroscopy. IFU spectroscopy provides spatially resolved kinematics, from which significantly improved $\sigma_\star$ determinations can be made, mitigating the effects of disk contamination and avoiding disproportionate sampling of galaxy substructure (e.g. bars). Our results can be summarized as follows.

(i) We find a best-fitting slope to the $M_{BH} - \sigma_\star$ relation of $\beta = 3.77 \pm 0.99$, with a scatter of $\epsilon = 0.35 \pm 0.17$. This is shallower than many recent fits to the quiescent galaxy sample, however it is consistent with recent investigations of the RM active galaxy sample.

(ii) We present a new determination of the virial factor,

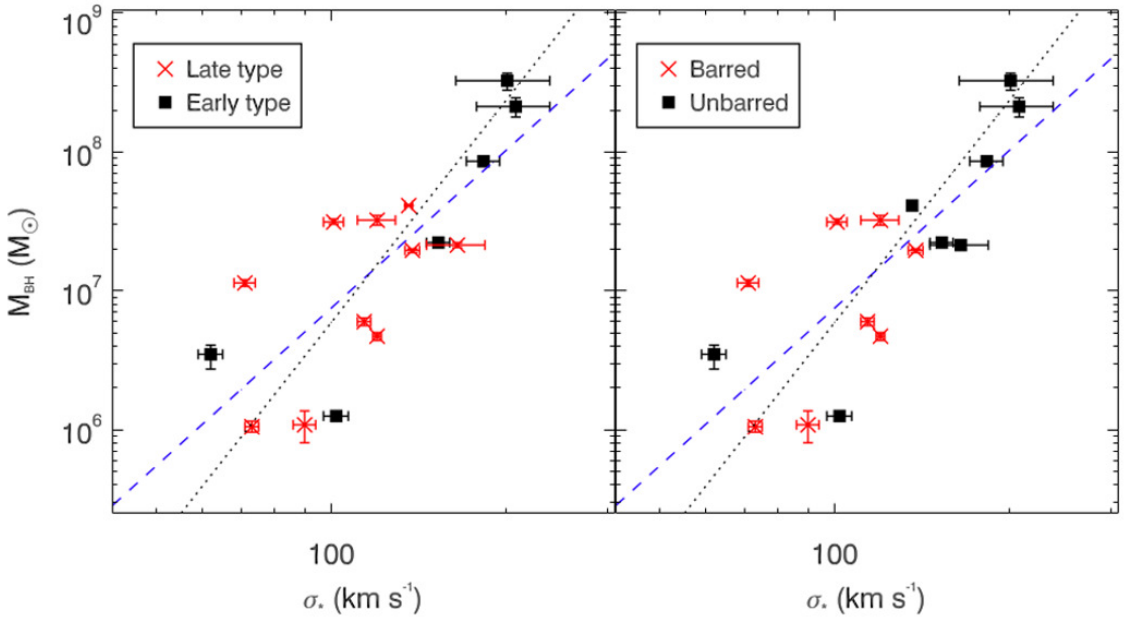

Figure 3. The $M_{BH} - \sigma_\star$ relation for the sample, with VP converted to M_{BH} using $f = 3.39$. The sample is separated into early- (squares) and late- (x) type galaxies in the left panel, and barred (x) and barless (squares) galaxies in the right panel. Our calculated best fit (scaled by f) is shown as the blue dashed line, and the fit for quiescent galaxies of Woo et al. (2013) is shown as the dotted line in both panels.

$f = 3.39 \pm 1.28$, which is lower than, but consistent with, previous investigations, as well as with results from direct modeling of the BLR.

(iii) We find no morphological dependence in the best-fitting $M_{BH} - \sigma_\star$ relation. There does appear to be higher scatter in this sample at the low mass end, however this may well result from sparse sampling at the high mass end of the relation, so a larger sample is required to confirm it.

ACKNOWLEDGMENTS

MCB gratefully acknowledges support from the NSF through CAREER grant AST-1253702 to Georgia State University.

REFERENCES

Bacon, R., Copin, Y., Monnet, G., et al. 2001, MNRAS, 326, 23
Batiste, M., Bentz, M. C., Manne-Nicholas, E. R., Onken, C. A., & Bershady, M. A. 2016, ApJ, submitted
Beifiori, A., Courteau, S., Corsini, E. M., & Zhu, Y. 2012, MNRAS, 419, 2497
Bellovary, J. M., Holley-Bockelmann, K., Gültekin, K., et al. 2014, MNRAS, 445, 2667
Bentz, M. C., Cackett, E. M., Crenshaw, D. M., et al. 2016a, ArXiv e-prints, arXiv:1608.01229
Bentz, M. C., & Katz, S. 2015, PASP, 127, 67
Bentz, M. C., Peterson, B. M., Netzer, H., Pogge, R. W., & Vestergaard, M. 2009, ApJ, 697, 160
Bentz, M. C., Denney, K. D., Grier, C. J., et al. 2013, ApJ, 767, 149
Bentz, M. C., Horenstein, D., Bazhaw, C., et al. 2014, ApJ, 796, 8
Bentz, M. C., et al. 2016b, in prep.
Blandford, R. D., & McKee, C. F. 1982, ApJ, 255, 419
Bonnet, H., Abuter, R., Baker, A., et al. 2004, The Messenger, 117, 17
Brown, J. S., Valluri, M., Shen, J., & Debattista, V. P. 2013, ApJ, 778, 151
Cappellari, M., & Emsellem, E. 2004, PASP, 116, 138
Cappellari, M., Emsellem, E., Krajnović, D., et al. 2011, MNRAS, 413, 813
Cappellari, M., Scott, N., Alatalo, K., et al. 2013, MNRAS, 432, 1709
Dopita, M., Hart, J., McGregor, P., et al. 2007, Ap&SS, 310, 255
Dopita, M., Rhee, J., Farage, C., et al. 2010, Ap&SS, 327, 245
Eisenhauer, F., Abuter, R., Bickert, K., et al. 2003, in Proc. SPIE, Vol. 4841, Instrument Design and Performance for Optical/Infrared Ground-based Telescopes, ed. M. Iye & A. F. M. Moorwood, 1548–1561
Ferrarese, L., & Merritt, D. 2000, ApJL, 539, L9
Gebhardt, K., Bender, R., Bower, G., et al. 2000, ApJL, 539, L13
Graham, A. W. 2008, ApJ, 680, 143
—. 2016, Galactic Bulges, 418, 263
Graham, A. W., Onken, C. A., Athanassoula, E., & Combes, F. 2011, MNRAS, 412, 2211
Grier, C. J., Martini, P., Watson, L. C., et al. 2013, ApJ, 773, 90
Gültekin, K., Richstone, D. O., Gebhardt, K., et al. 2009, ApJ, 698, 198
Hartmann, M., Debattista, V. P., Cole, D. R., et al. 2014, MNRAS, 441, 1243
Hu, J. 2008, MNRAS, 386, 2242
Kelly, B. C. 2007, ApJ, 665, 1489
Kormendy, J., & Ho, L. C. 2013, ARA&A, 51, 511
Krajnović, D., Emsellem, E., Cappellari, M., et al. 2011, MNRAS, 414, 2923
McConnell, N. J., & Ma, C.-P. 2013, ApJ, 764, 184
McGregor, P. J., Hart, J., Conroy, P. G., et al. 2003, in Proc. SPIE, Vol. 4841, Instrument Design and Performance for Optical/Infrared Ground-based Telescopes, ed. M. Iye & A. F. M. Moorwood, 1581–1591
Onken, C. A., Ferrarese, L., Merritt, D., et al. 2004, ApJ, 615, 645
Pancoast, A., Brewer, B. J., Treu, T., et al. 2014, MNRAS, 445, 3073
Park, D., Kelly, B. C., Woo, J.-H., & Treu, T. 2012, ApJS, 203, 6
Peng, C. Y., Ho, L. C., Impey, C. D., & Rix, H.-W. 2002, AJ, 124, 266
—. 2010, AJ, 139, 2097
Raimundo, S. I., Davies, R. I., Gandhi, P., et al. 2013, MNRAS, 431, 2294
Savorgnan, G. A. D., & Graham, A. W. 2015, MNRAS, 446, 2330

Shankar, F., et al. 2016, MNRAS, 460, 3119
van den Bosch, R. 2016, ArXiv e-prints, arXiv:1606.01246
Williams, M. J., Bureau, M., & Cappellari, M. 2010, MNRAS, 409, 1330
Woo, J.-H., Schulze, A., Park, D., et al. 2013, ApJ, 772, 49
Woo, J.-H., Yoon, Y., Park, S., Park, D., & Kim, S. C. 2015, ApJ, 801, 38
Woo, J.-H., Treu, T., Barth, A. J., et al. 2010, ApJ, 716, 269
Wood, C. M., Bershady, M. A., Eigenbrot, A. D., et al. 2012, in Proc. SPIE, Vol. 8446, Ground-based and Airborne Instrumentation for Astronomy IV, 84462W